IEEE Access
Multidisciplinary | Rapid Review | Open Access Journal

Received November 9, 2021, accepted December 4, 2021, date of publication December 20, 2021, date of current version January 20, 2022.

Digital Object Identifier 10.1109/ACCESS.2021.3136612

Flight-Propulsion Integration Dynamic Analysis and Adaptive Control of the Hypersonic Vehicle at Wide-Range Mach Numbers

JIAXIN LI[1,2], DANWEI LI[3], GUOQIANG WU[1,2], AND KAI LIU[1,2]

[1]Key Laboratory of Advanced Technology for Aerospace Vehicles, Dalian University of Technology, Dalian 116024, China
[2]School of Aeronautics and Astronautics, Dalian University of Technology, Dalian 116024, China
[3]Shenyang Aircraft Design and Research Institute, Shenyang 110000, China

Corresponding author: Danwei Li (dwli10000@163.com)

This work was supported in part by the National Natural Science Foundation of China under Grant NSFC U2141229.

ABSTRACT There are serious among various components of the hypersonic vehicle at wide-range Mach numbers, and the coupling among aerodynamic shape, propulsion system, structure, and control system is remarkable. For excellent performance, its components and functions are highly integrated, which brings serious challenges to traditional design examples, methods, and tools. To solve the integrated control problem of flight-propulsion coupling, a controller based on pole assignment is designed in this paper, and the control parameters can be adjusted according to real-time aerodynamic data. The parametric model of hypersonic vehicle at wide-range Mach numbers with coupling characteristics is established and the flight data under various working conditions are obtained. The flight dynamical model is established with a coupling relationship between the airframe and engine. Combined with the characteristic parameters of the aircraft attitude control closed-loop system, the control gain is designed based on expected poles and adjusted in real-time. The comparative simulations are carried out, and the results show that the control gain adjustment strategy based on aerodynamic parameter identification can improve the attitude angle command tracking quality and the robustness of the system.

INDEX TERMS Hypersonic vehicle, wide-range Mach numbers, aerodynamic parameter identification, coupling control, control gain adjustment strategy.

I. INTRODUCTION

The hypersonic vehicle at wide-range Mach numbers refers to an aircraft whose flying Mach number is greater than 5, using a scramjet engine and its combined power, capable of maneuvering in the adjacent space at a height of 20-100km from sea level and relying on a rare atmosphere to perform missions such as strikes, investigations, carrying and confrontation [1]–[4]. With characteristics of high flight speed, rapid response, wide speed range, large lift-drag ratio, and big specific impulse, it shows remarkable advantages compared with conventional aircraft and has important military and civil value.

The scramjet engine has the characteristics of multivariable, non-linear, and time-varying which takes the difficulty to its control system. The coupling and mutual influence of aerodynamic force, engine working state of the hypersonic vehicle at wide-range Mach numbers are mainly expressed in that the flight attitude affects the thrust by the air mass flow rate of the inlet [5]–[7]. Meanwhile, thrust affects hypersonic vehicle attitude in two aspects. First, due to the special structure of the combined power engine, the thrust center can't be set at the centroid position of aircraft, which brings about an eccentric moment. Second, the high-speed expansion airflow from the nozzle acts on the asymmetric outer nozzle, resulting in an additional moment. Therefore, the coordinated control of attitude, speed, and thrust is particularly important [7]–[9]. Because of the particularity of the wide-range velocity vehicle, the conventional strategy usually used for the control system is not suitable for the application [10]. During the flight of an aircraft in a large altitude and speed range, the aerodynamic and thrust coefficients will change nonlinearly, which also brings challenges to flight control.

The associate editor coordinating the review of this manuscript and approving it for publication was Zijian Zhang.

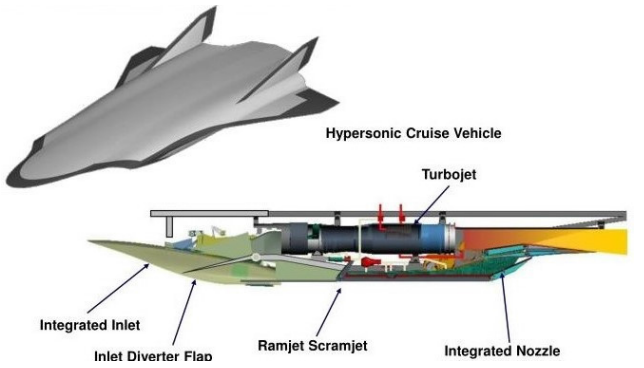

FIGURE 1. Hypersonic vehicle.

The National Aeronautics and Space Administration (NASA) developed the ''Learn-to-fly''(L2F) algorithm, in the Transforming Aviation Concept Program (TACP), with the purpose to update the development model of aircraft. The traditional aircraft development process includes wind tunnel tests, aero-fluid dynamics calculations (CFD), simulation development, control law design, and the final flight test sequence, and iterates continuously [11]–[13]. Inevitably, during the flight test, the aerodynamic model needs to be continuously updated. Whenever the aerodynamic model needs to be updated, the development process will be iterated once. L2F combines real-time nonlinear aerodynamic modeling with autonomous control law design. The advantages of L2F include the use of aerodynamic models based on real-time identification of flight data in the control law design. Therefore, there is no need to modify the Reynolds number, blockage, boundary layer turbulence, etc., [14]–[16]. The control system design is developed based on the actual flight dynamics response rather than the simulation results. As L2F technology matures, new aircraft designs may not require the ground test [17]–[19]. The three pillars of L2F theory are the hot spots of research in recent years: 1) real-time nonlinear aerodynamic modeling; 2) ''learning'' control law design method; 3) guidance algorithm. In the L2F research, the flight test aerodynamic modeling method is combined with the real-time guidance and learning control law design method on the aircraft and applied in flight. These technologies enable the aircraft to learn how to fly [20], [22].

Many scholars besides NASA have also made thorough research on the control of the hypersonic vehicle at wide-range Mach numbers. In Refs. [22] and [23], several original contributions were made by X. W. and Q. Qi, who developed a fuzzy optimal tactic which deals with the tracking control problem of the hypersonic vehicle subject to unknown dynamics. Recently, they made an effort to apply a simplified finite-time fuzzy neural controller with prescribed performance to waverider aircraft which could guarantee satisfied real-time performance with low-complex structure. X. Bu presented a funnel non-affine controller applying neural approximation for prescribed tracking of air-breathing hypersonic vehicles. The desired transient performance and steady-state performance are ensured for both tracking errors [24].

Trajectory Linearization Control (TLC) is a nonlinear control method based on differential-algebraic spectrum theory, which has been applied to the design of X-33's ascent attitude control system in NASA's advanced guidance and control project. It is an advanced control method for hypersonic vehicle control at present [25]. TLC and PID will be performed as comparative groups, reflecting the control effect of the adaptive integration method based on the desired pole assignment.

In this paper, the real-time aerodynamic and thrust data of aircraft are obtained based on the parametric model of the hypersonic vehicle at wide-range Mach numbers. A comprehensive control algorithm based on pole assignment is adopted. On the premise of knowing the real-time aerodynamic parameters of the aircraft, combined with the concept of learning flight, it is hoped that the interaction in flight dynamics, aerodynamics, thermodynamics, frequency and dynamics of the control system of the hypersonic vehicle at wide-range Mach numbers can be handled with a low-complex control structure, which is expected to improve the control quality.

The contributions of this paper mainly include the following four points:

The parametric model of hypersonic vehicle at wide-range Mach numbers is constructed and the flight data under various working conditions are calculated.

The adaptive controller design based on the expected pole assignment is completed.

According to the aerodynamic real-time identification results, the state feedback matrix is designed.

The comparative simulation is completed, and the algorithm to solve the aerodynamic/thrust coupling problem is verified.

This paper is structured as follows: In section 2, the mathematical model and the essential method of aerodynamic and propulsion characteristics analysis of the hypersonic vehicle at wide-range Mach numbers are expounded. The dynamic analysis of the hypersonic vehicle at wide-range Mach numbers is carried out in section 3. Section 4 describes the control scheme based on pole assignment and the adaptive control gain compensation method. Section 5 gives the simulation comparison results and section 6 gives discussion.

II. THE HYPERSONIC VEHICLE AT WIDE-RANGE MACH NUMBERS MODEL

A. AERODYNAMIC AND PROPULSION CHARACTERISTICS ANALYSIS

Parametric models of aircraft need to be established before aerodynamic and thrust analysis [26]–[30]. In aerodynamic estimation, the panel method is adopted, and its basic idea is to divide the surface of the hypersonic vehicle at wide-range Mach numbers into several small areas and replace them with a parallelogram or triangle. The aerodynamic forces and moments on the panels are calculated, and the total aerodynamic forces and moments are obtained by adding the

calculated results. Identifying a panel need to determine the centroid coordinates, direction, and area. The quadrilateral panel is used for specific explanations.

The coordinates of the four vertices of the quadrilateral panel are Q_1, Q_2, Q_3, Q_4, and the normal vector outside the panel is calculated by:

$$\mathrm{n} = \frac{T_1 \times T_2}{\|T_1 \times T_2\|} \tag{1}$$

where T_1, T_2 are the vector obtained by subtracting the coordinates of two groups of non-adjacent points.

The panel plane can be determined by the normal vector of the panel and the center of the panel. The four vertices are projected to the panel plane, and the points projected on the panel plane are called "corners". The coordinates of the four corners are:

$$\begin{cases} P_i' = P_i + d_i \vec{n} \\ d_i = \vec{n}\left(\bar{P} - P_i\right) \end{cases} \tag{2}$$

where $\bar{P}$ is the median coordinate of 4 nodes. The coordinate system is established based on the panel, the origin is in the center of the panel, and the three axial directions are: $i_p = T_1/|T_1|, j_p = n \times n_x, k_p = n$. The transformation from computational coordinate system to panel coordinate system:

$$R_{cp} = \left[i_p, j_p, k_p\right] \tag{3}$$

The coordinates of the four corners in the panel coordinate system are as follows:

$$\tilde{P}_i = R_{cp}^T\left(P_i' - P_i\right) \tag{4}$$

The coordinates of that centroid of the panel in the panel coordinate system are as follows:

$$\begin{aligned} \bar{P}_x' &= \frac{1}{3}\frac{1}{\tilde{P}_{2y} - \tilde{P}_{4y}}\left[\tilde{P}_{4x}\left(\tilde{P}_{1y} - \tilde{P}_{2y}\right) + \tilde{P}_{2x}\left(\tilde{P}_{4y} - \tilde{P}_{1y}\right)\right] \\ \bar{P}_y' &= -\frac{1}{3}\tilde{P}_{1y} \\ \bar{P}_z' &= 0 \end{aligned} \tag{5}$$

The coordinate of that centroid of the panel in the calculated coordinate system is as follow:

$$P_{cg} = \bar{P} + S'\begin{bmatrix} \bar{P}_x' \\ \bar{P}_y' \\ \bar{P}_z' \end{bmatrix} \tag{6}$$

The area of the panel is:

$$S = \left(\tilde{P}_{3x} - \tilde{P}_{1x}\right)\left(\tilde{P}_{2y} - \tilde{P}_{4y}\right)/2 \tag{7}$$

According to the engineering estimation method, the pressure on the ith plane is obtained.

$$P_i = C_{pi} q_{c,i} + P_\infty \tag{8}$$

P_∞ is local static pressure and $q_{c,i}$ is local dynamic pressure.

The total aerodynamic force and aerodynamic moment on the aircraft can be obtained by adding the aerodynamic force and aerodynamic moment vectors on all panels.

$$\begin{cases} F_{a,x} = -\sum P_i n_{xi} S_{pan,i} \\ F_{a,y} = -\sum P_i n_{yi} S_{pan,i} \\ F_{a,z} = -\sum P_i n_{zi} S_{pan,i} \end{cases} \tag{9}$$

$$\begin{cases} M_{a,x} = \sum P_i\left(d_{zi} n_{yi} - d_{yi} n_{zi}\right) S_{pan,i} \\ M_{a,y} = \sum P_i\left(d_{xi} n_{zi} - d_{zi} n_{xi}\right) S_{pan,i} \\ M_{a,z} = \sum P_i\left(d_{yi} n_{xi} - d_{xi} n_{yi}\right) S_{pan,i} \end{cases} \tag{10}$$

In which, $d_i = d_{xi} i_b + d_{yi} j_b + d_{zi} k_b$ is the distance vector from the centroid of the panel to the centroid of aircraft, and n_{xi}, n_{yi}, n_{zi} are the components of n on i_b, j_b, k_b.

$$\begin{cases} F_{a,x} = -F_{a,x}\dfrac{1}{q_c S_{ref}} \\ F_{a,y} = -F_{a,y}\dfrac{1}{q_c S_{ref}} \\ F_{a,z} = -F_{a,z}\dfrac{1}{q_c S_{ref}} \end{cases} \tag{11}$$

$$\begin{cases} C_{m,ax} = -M_{a,x}\dfrac{1}{q_c S_{ref} l_{ref}} \\ C_{m,ay} = -M_{a,y}\dfrac{1}{q_c S_{ref} l_{ref}} \\ C_{m,az} = -M_{a,z}\dfrac{1}{q_c S_{ref} l_{ref}} \end{cases} \tag{12}$$

The panel effect of airfoils is shown in Figure 2. Each small panel is represented by a small arrow pointing to its normal vector. The red part is the elevator, which can deflect with the input angle.

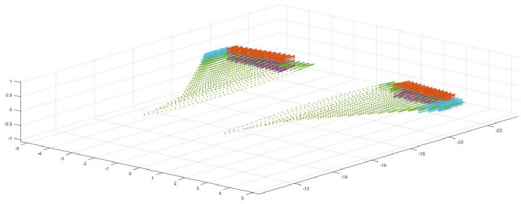

FIGURE 2. Panels generation effect.

The pressure and pressure coefficient of each small panel are calculated by using the Modified Newton method (Formula 13-14) and the Prandtl-Meyer method (Formula 15), and the total aerodynamic force and aerodynamic moment under this working condition can be obtained by adding the vectors of each panel. Where γ_e is the specific heat ratio of fuel and τ is the impact angle of airflow [31]–[33]. (13)–(15), as shown at the bottom of the next page.

In thrust estimation, scramjet is divided into the inlet, isolator, combustion chamber, and nozzle.

In the inlet part, shock wave, expansion wave, and their intersection theory are used to describe the flow parameters. All of the shock waves and expansion waves in the flow region produced by the turning of the inlet surface

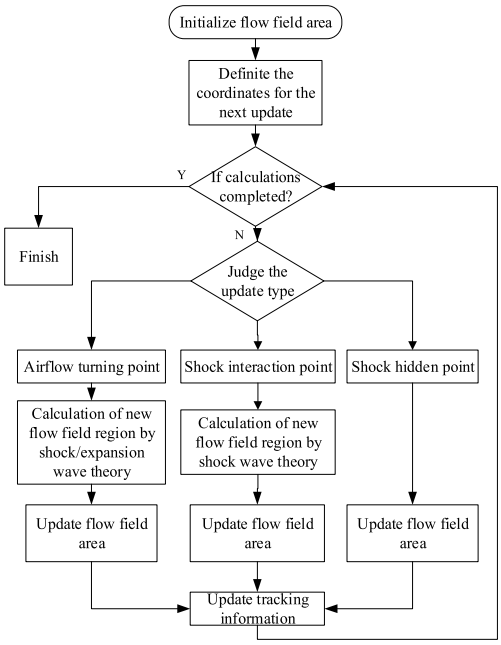

FIGURE 3. The flow calculation process of quasi-two-dimensional inlet.

and the intersection of shock waves and expansion waves are calculated. These waves divide the two-dimensional area into several small areas. The internal airflow parameters in each small area remain constant, which are determined by the shock waves or expansion waves in front. If there is a detached shock wave or the calculated wave surface is more than a certain number, the average airflow parameters here will be calculated instead. The airflow parameters from here to the isolation section can be determined according to the frictional variable cross-section pipe flow formula (formula 16). The algorithm flow is shown in Figure 3.

$$\begin{cases} \dfrac{dMa}{dx} = \dfrac{Ma\psi_{th}}{1-Ma^2}\left(-\dfrac{1}{S_{th}}\dfrac{dS_{th}}{dx} + \gamma_c Ma^2\dfrac{2C_f}{d_{th}}\right) \\ \dfrac{dP}{dx} = \dfrac{P\gamma_c Ma^2}{1-Ma^2}\left(\dfrac{1}{S_{th}}\dfrac{dS_{th}}{dx} - \dfrac{1+(\gamma_c-1)Ma^2}{2}\dfrac{4C_f}{d_{th}}\right) \\ \dfrac{dT}{dx} = \dfrac{(1-\gamma_c)TMa^2}{1-Ma^2}\left(\dfrac{1}{S_{th}}\dfrac{dS_{th}}{dx} + \gamma_c Ma^2\dfrac{2C_f}{d_{th}}\right) \end{cases} \tag{16}$$

where: S_{th} is the cross-sectional area of the airflow channel and d_{th} is the hydraulic diameter, $\psi_{th} = 1 + Ma^2(\gamma_c - 1)/2$.

The quasi-one-dimensional model is adopted to calculate the airflow parameters in the isolation section and combustion chamber, and the airflow friction, fuel injection, length change of pre-combustion shock wave train, reaction rate are out of consideration. The basic conservation equations of airflow in the isolation section and combustion chamber are obtained, and the equations need to combine experimental or empirical formulas to get solved. Finally, the airflow parameter distribution law in the isolation section and combustion chamber is [34], [35]:

$$\frac{dMa}{dx} = \frac{Ma\psi_{th}}{1-Ma^2}\left[\begin{array}{c} -\dfrac{1}{S_{th}}\dfrac{dS_{th}}{dx} + \dfrac{1+\gamma_c Ma^2}{2T_t}\dfrac{dT_t}{dx} + \\ \dfrac{1+\gamma_c Ma^2-\varepsilon_{th}\gamma_c Ma^2}{\dot{m}_{ad}}\dfrac{d\dot{m}_{ad}}{dx} + \gamma_c Ma^2\dfrac{2C_f}{d_{th}} \end{array}\right] \tag{17}$$

$$\frac{dP}{dx} = \frac{P\gamma_c Ma^2}{1-Ma^2}\left[\begin{array}{c} \dfrac{1}{S_{th}}\dfrac{dS_{th}}{dx} - \dfrac{\psi_{th}}{T_t}\dfrac{dT}{dx} - \dfrac{2\psi_{th}(1-\varepsilon)+\varepsilon_{th}}{\dot{m}_{ad}}\dfrac{d\dot{m}_{ad}}{dx} \\ -\dfrac{1+(\gamma_c-1)Ma^2}{2}\dfrac{4C_f}{d_{th}} \end{array}\right] \tag{18}$$

$$\frac{dT}{dx} = \frac{1}{\psi_{th}}\frac{dT_t}{dx} - \frac{(\gamma_c-1)TMa}{\psi_{th}}\frac{dMa}{dx} \tag{19}$$

In which: S_{th}, dS_{th}/dx and d_{th} can be determined by the engine combustion chamber geometry; $\dot{m}_{ad}$ and $d\dot{m}_{ad}/dx$ are respectively the fuel mass flow rate and the fuel mass flow rate change rate added into the combustion chamber, ε_{th} is the ratio of the fuel injection speed on the engine shaft of the aircraft to the main airflow speed, and can be determined according to the fuel injection.

$$C_p = K\sin^2\tau \tag{13}$$

$$K = \frac{2}{\gamma_e Ma^2}\left\{\left[\frac{(\gamma_e+1)^2 Ma^2}{4\gamma_e Ma^2 - 2(\gamma_e-1)}\right]^{\frac{\gamma_e}{\gamma_e-1}}\left[\frac{1-\gamma_e+2\gamma_e Ma^2}{\gamma_e+1}\right] - 1\right\} \tag{14}$$

$$C_p = \begin{cases} -\dfrac{(\gamma_e+1)\tau^2}{2}\left\{\sqrt{1+\left[\dfrac{4}{(\gamma_e+1)Ma\tau}\right]^2} - 1\right\} & Ma > Ma_2 \\ -\dfrac{(\gamma_e+1)\tau^2(Ma-6.5)^2}{8}\left\{\sqrt{1+\left[\dfrac{8}{(\gamma_e+1)Ma\tau\,(Ma-6.5)}\right]^2} - 1\right\} & Ma_1 < Ma < Ma_2 \\ 0 & Ma < Ma_1 \end{cases} \tag{15}$$

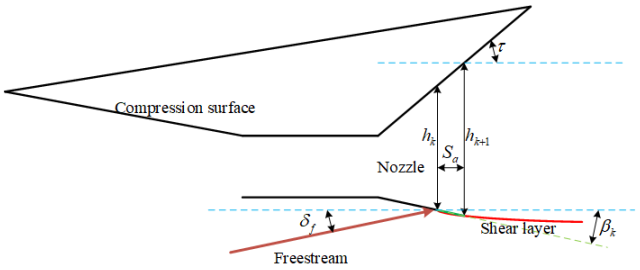

FIGURE 4. The nozzle plume model.

The plume method is adopted at the nozzle reflecting the coupling of flight and propulsion [36], [37]. The plume model is based on the equal air pressure above and below the shear layer (see Fig 3).

$$h_{k+1} = h_k + s_a \tan(\tau) + s_a \tan(\beta_k) \tag{20a}$$

$$A_k = h_{k+1}/h_k \tag{20b}$$

$$f(M_k) = 1 + \frac{1}{2}(\gamma - 1)M_k^2 \tag{20c}$$

$$\frac{f(M_k)^{\frac{\gamma+1}{\gamma-1}}}{M_k^2} = A_k^2 \frac{f(M_{k-1})^{\frac{\gamma+1}{\gamma-1}}}{M_{k-1}^2} \tag{20d}$$

$$P_k = P_{k-1}\left[\frac{f(M_{k-1})}{f(M_k)}\right]^{\frac{\gamma}{\gamma-1}} \tag{20e}$$

$$\bar{P}_k = \bar{\rho}_e \bar{V}_e^2 \sin^2\left(\beta_k - \delta_f\right) + \bar{P}_e \tag{20f}$$

$$\bar{P}_k - P_k = 0 \tag{20g}$$

$\bar{P}_e$ is the fluid pressure under the shear layer. $\bar{\rho}_e$ is the fluid density under the shear layer. $\bar{V}_e$ is the fluid velocity under the shear layer.

B. DYNAMIC MODEL OF THE HYPERSONIC VEHICLE AT WIDE-RANGE MACH NUMBERS

The force of the hypersonic vehicle is divided into three categories: one: vertical downward gravity, two: thrust in the direction of the body axis, three: aerodynamic force, the aerodynamic force is decomposed into a lift perpendicular to the speed, and the resistance is opposite to the speed direction. Combined with Newton's law, the following equations can be obtained. The system of equations describes the relationship between the force of the hypersonic vehicle at wide-range Mach numbers and the displacement of the longitudinal channel and flight attitude. The control is based on this system of equations.

$$\begin{cases} \dot{x} = V\cos\theta\cos\psi_v \\ \dot{H} = V\sin\theta \\ \dot{z} = -V\cos\theta\sin\psi_v \end{cases} \tag{21}$$

$$\begin{cases} \dot{\vartheta} = \omega_y\sin\gamma + \omega_z\cos\gamma \\ \dot{\psi} = \left(\omega_y\cos\gamma - \omega_z\sin\gamma\right)/\cos\vartheta \\ \dot{\gamma} = \omega_x - \tan\vartheta\left(\omega_y\cos\gamma - \omega_z\sin\gamma\right) \end{cases} \tag{22}$$

$$\begin{cases} \dot{\omega}_x = \left(I_{yy}M_x + I_{xy}M_y\right)\Big/\left(I_{xx}I_{yy} - I_{xy}^2\right) \\ \dot{\omega}_y = \left(I_{xy}M_x + I_{xx}M_y\right)\Big/\left(I_{xx}I_{yy} - I_{xy}^2\right) \\ \dot{\omega}_z = M_z/I_{zz} \end{cases} \tag{23}$$

where α is the angle of attack; ϑ is the pitch angular, β is the angle of sideslip, γ_V is the velocity inclination angle, ψ is the yawing angle, ψ_V is the velocity declination; ω is the angular rate; L, T, D are lift force, thrust, and drag; M is pitch moments; I is pitch moments of inertial; V, m, g, θ are velocity, vehicle mass, gravity acceleration, the flight path angle; M is the moment, in which longitudinal moment is divided into aerodynamic pitch moment M_A and thrust pitch moment M_T;

III. DYNAMIC CHARACTERISTIC ANALYSIS

A. DYNAMIC CHARACTERISTIC VERIFICATION OF PARAMETRIC MODEL

Validating the effectiveness of the developed model is an essential step to ensure the developed model is reliable. In this part, the trim capacity of lift to gravity and thrust to drag is put to the proof. The trim elevator deflection at each angle of attack is also a key concern. The thrust eccentricity, the additional moment generated by the internal flow on the afterbody flow field and the balancing of the external aerodynamic moment are taken into consideration. The static stability analysis under the equilibrium characteristic points is carried out, and the corresponding static stability coefficients and maneuverability at different angles of attack are solved respectively. It is proved that the model is reliable and can be applied to control.

Form Figs. 5(a-e), we can conclude that:

1) the drag reaches the minimum near the angle of attack of 0 degrees, and the fuel equivalent ratio has no prominent influence on the drag. The thrust increases with the increase of angle of attack or fuel equivalence

$$\begin{cases} \dot{V} = \left(T\cos\alpha\cos\beta - D - mg\sin\theta\right)/m \\ \dot{\theta} = \left[T\left(\sin\alpha\cos\gamma_v + \cos\alpha\sin\beta\sin\gamma_v\right) + L\cos\gamma_v - Z\sin\gamma_v - mg\cos\theta\right]/(mV) \\ \dot{\psi}_v = -\left[T\left(\sin\alpha\sin\gamma_v - \cos\alpha\sin\beta\cos\gamma_v\right) + L\sin\gamma_v + Z\cos\gamma_v\right]/(mV\cos\theta) \end{cases} \tag{24}$$

$$\begin{cases} \sin\beta = \cos\theta\left[\cos\gamma\sin\left(\psi - \psi_v\right) + \sin\vartheta\sin\gamma\cos\left(\psi - \psi_v\right)\right] - \sin\theta\cos\vartheta\sin\gamma \\ \sin\alpha = \left\{\cos\theta\left[\sin\vartheta\cos\gamma\cos\left(\psi - \psi_v\right) - \sin\gamma\sin\left(\psi - \psi_v\right)\right] - \sin\theta\cos\vartheta\cos\gamma\right\}/\cos\beta \\ \sin\gamma_v = \left(\cos\alpha\sin\beta\sin\vartheta - \sin\alpha\sin\beta\cos\gamma\cos\vartheta + \cos\beta\sin\gamma\cos\vartheta\right)/\cos\theta \end{cases} \tag{25}$$

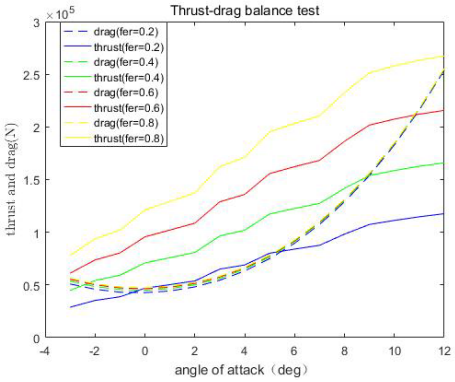

(a)

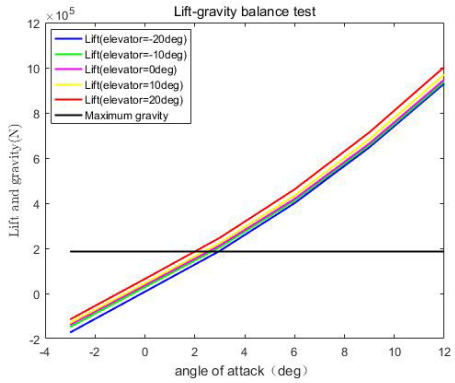

(b)

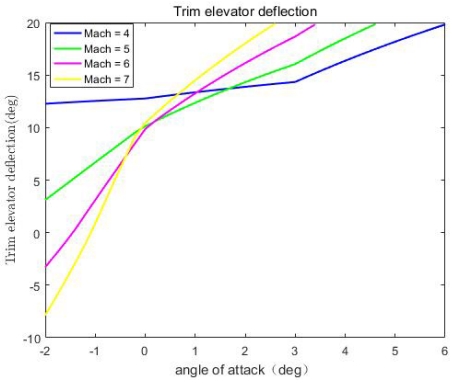

(c)

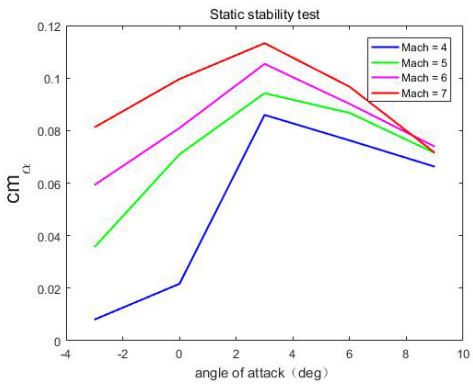

(d)

FIGURE 5. Model validation chart. (a) Thrust-drag balance test; (b) Lift-gravity balance test; (c) Trimming rudder deflection at different angles of attack and Mach number; (d) Static stability test; (e) Elevator efficiency test.

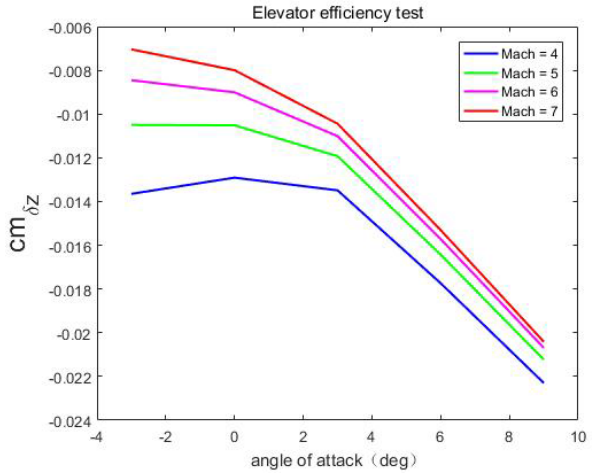

(e)

FIGURE 5. *(Continued.)* Model validation chart. (a) Thrust-drag balance test; (b) Lift-gravity balance test; (c) Trimming rudder deflection at different angles of attack and Mach number; (d) Static stability test; (e) Elevator efficiency test.

ratio, which shows that the developed model has trim capability in a large angle of attack range.

2) The lift can be balanced with the maximum gravity near the angle of attack of three degrees.
3) The trim ability of the elevator decreases with the increase of Mach number, but the pitching moment can be trimmed within a reasonable angle of attack.
4) The developed model between Ma4-6 is statically unstable, and the maximum static instability is near 3 degrees angle of attack.
5) The elevator efficiency of the developed model is within a reasonable range.

B. FLIGHT MECHANICS ANALYSIS

Undisturbed motion is space unsteady flight, and the missile motion equation is linearized with small disturbance:

$$\begin{aligned}
\frac{d\Delta V}{dt} &= \frac{\left(P^V - X^V\right)}{m}\Delta V + \frac{\left(P^\alpha - P\alpha - X^\alpha\right)}{m}\Delta\alpha \\
&\quad + \frac{\left(P^\varphi - X^\varphi\right)}{m}\Delta\varphi - \frac{X^{\delta_z}}{m}\Delta\delta_z - \Delta\theta g\cos\theta + \frac{F_{gx}}{m} \\
\frac{d\Delta\theta}{dt} &= \frac{\left(P^V\alpha + Y^V\right)}{mV}\Delta V + \frac{\left(P^\alpha\alpha + P + Y^\alpha\right)}{mV}\Delta\alpha \\
&\quad + \frac{\left(P^\varphi\alpha + Y^\varphi\right)}{mV}\Delta\varphi + \frac{g\sin\theta}{V}\Delta\theta + \frac{Y^{\delta_z}}{mV}\Delta\delta_z + \frac{F_{gy}}{m} \\
\frac{d\Delta\omega_z}{dt} &= \left(\frac{M_z^V}{J_z} + \frac{M_{th}^V}{J_z}\right)\Delta V + \left(\frac{M_z^\alpha}{J_z} + \frac{M_{th}^\alpha}{J_z}\right)\Delta\alpha \\
&\quad + \frac{M_z^{\omega_z}}{J_z}\Delta\omega_z + \frac{M_z^{\delta_z}}{J_z}\Delta\delta_z + \frac{M_{th}^\varphi}{J_z}\Delta\varphi + \frac{M_{gx}}{m} \\
\frac{d\Delta\varphi}{dt} &= \varphi^V\Delta V + \varphi^\alpha\Delta\alpha + \varphi^{\varphi_c}\Delta\varphi_c + \varphi_g \\
\frac{d\Delta I_\varphi}{dt} &= \varphi
\end{aligned} \tag{26}$$

TABLE 1. Symbol of dynamic coefficient and its expression.

1	2	3	4
$a_{11}=\dfrac{P^V-X^V}{m}$	$a_{21}=\left(\dfrac{M_z^V}{J_z}+\dfrac{M_{th}^V}{J_z}\right)$	$a_{31}=\dfrac{P^V\alpha+Y^V}{mV}$	$a_{41}=\dfrac{\frac{\partial d\dot{M}as}{\partial V}dMas-\frac{\partial dMas}{\partial V}d\dot{M}as}{dMas^2}\times\varphi$
$a_{12}=0$	$a_{22}=\dfrac{M_z^{\omega_z}}{J_z}$	$a_{32}=0$	$a_{42}=0$
$a_{13}=-g\cos\theta$	$a_{23}=0$	$a_{33}=\dfrac{g\sin\theta}{V}$	$a_{43}=0$
$a_{14}=\dfrac{P^\alpha-P\alpha-X^\alpha}{m}$	$a_{24}=\left(\dfrac{M_z^\alpha}{J_z}+\dfrac{M_{th}^\alpha}{J_z}\right)$	$a_{34}=\dfrac{P^\alpha\alpha+P+Y^\alpha}{mV}$	$a_{44}=\dfrac{\frac{\partial d\dot{M}as}{\partial \alpha}dMas-\frac{\partial dMas}{\partial \alpha}d\dot{M}as}{dMas^2}\times\varphi$
$a_{15}=\dfrac{-X^{\delta_z}}{m}$	$a_{25}=\dfrac{M_z^{\delta_z}}{J_z}$	$a_{35}=\dfrac{Y^{\delta_z}}{mV}$	$a_{45}=0$
$a_{16}=\dfrac{P^\varphi-X^\varphi}{m}$	$a_{26}=\dfrac{M_{th}^\varphi}{J_z}$	$a_{26}=\dfrac{P^\varphi\alpha+Y^\varphi}{mV}$	$a_{46}=0$
$a_{17}=0$	$a_{27}=0$	$a_{37}=0$	$a_{47}=K\omega_n$

To make the above formula easy to write, the simplified symbol of the equation coefficient is introduced.

a_{24} can represent the static stability of aircraft. If $a_{24}<0$, the aircraft is statically stable, otherwise it is statically unstable. a_{25} can represent the maneuverability of the aircraft, that is, the moment change that can be produced when the elevator deflects by one unit.

The free disturbance motion of the hypersonic vehicle at wide-range Mach numbers is analyzed, and the free disturbance motion equations are obtained by $\Delta\delta_z=0$, $\Delta\varphi_c=0$, $F_{gx}=F_{gy}=M_{gx}=0$ in Equation 27.

$$\begin{aligned}
\frac{d\Delta V}{dt}-a_{11}\Delta V-a_{13}\Delta\theta-a_{14}\Delta\alpha-a_{16}\Delta\varphi&=0\\
-a_{21}\Delta V+\frac{d^2\Delta\vartheta}{dt}-a_{22}\frac{d\Delta\vartheta}{dt}-a_{24}\Delta\alpha-a_{26}\Delta\varphi&=0\\
-a_{31}\Delta V-a_{33}\Delta\theta+\frac{d\Delta\theta}{dt}-a_{34}\Delta\alpha-a_{36}\Delta\varphi&=0\\
\frac{d\Delta\varphi}{dt}-a_{41}\Delta V-a_{44}\Delta\alpha&=0\\
-\Delta\vartheta+\Delta\theta+\Delta\alpha&=0
\end{aligned}\tag{27}$$

The following special solutions $\Delta V=Ae^{\lambda t}$, $\Delta\vartheta=Be^{\lambda t}$, $\Delta\theta=Ce^{\lambda t}$, $\Delta\alpha=De^{\lambda t}$, $\Delta\varphi=Ee^{\lambda t}$ in the form of exponential functions of the equations are: $\frac{d\Delta V}{dt}=A\lambda e^{\lambda t}$, $\frac{d\Delta\vartheta}{dt}=B\lambda e^{\lambda t}$, $\frac{d^2\Delta\vartheta}{dt^2}=B\lambda^2e^{\lambda t}$, $\frac{d\Delta\theta}{dt}=C\lambda e^{\lambda t}$, $\frac{d\Delta\alpha}{dt}=\lambda De^{\lambda t}$, $\frac{d\Delta\varphi}{dt}=\lambda Ee^{\lambda t}$. After eliminating the common term, the dynamic stability of aircraft can be judged by solving the characteristic equation.

Ignore the velocity which changes in a long period. The transfer function matrix in a short period is given.

$$\mathbf{G}(s)=\mathbf{C}\begin{bmatrix}s(s-a_{22})&0&-a_{24}&-a_{26}\\0&s-a_{33}&-a_{34}&-a_{36}\\0&0&-a_{44}&s\\-1&1&1&0\end{bmatrix}^{-1}\times\begin{bmatrix}a_{25}&0\\a_{35}&0\\0&a_{47}\\0&0\end{bmatrix}\tag{28}$$

where

$$\mathbf{C}=\begin{bmatrix}1&0&0&0\\0&1&0&0\\0&0&1&0\\0&0&0&1\end{bmatrix}.$$

IV. ADAPTIVE CONTROL BASED ON POLE ASSIGNMENT

According to the longitudinal short-period disturbance motion $\Delta\dot{V}=\Delta V\approx 0$, from the time domain point of view, the state vector $\left[\omega_z\ \alpha\ \varphi\ I_\varphi\right]^{\mathrm{T}}$ is adopted: the standard expression form of the longitudinal disturbance motion state space is:

$$\begin{bmatrix}\dot{\omega}_z\\\dot{\alpha}\\\dot{I}_\varphi\\\dot{\varphi}\end{bmatrix}=\mathbf{A}_z\begin{bmatrix}\omega_z\\\alpha\\I_\varphi\\\varphi\end{bmatrix}+\begin{bmatrix}a_{25}&0\\-a_{35}&0\\0&0\\0&a_{47}\end{bmatrix}\begin{bmatrix}\delta_z\\\varphi_c\end{bmatrix}+\begin{bmatrix}M_{zd}\\-F_{yd}\\I_{\varphi d}\\\varphi_d\end{bmatrix}\tag{29}$$

where:

$$\mathbf{A}_z = \begin{bmatrix} a_{22} & a_{24} & 0 & a_{26} \\ 1 & a_{33} - a_{34} & 0 & -a_{36} \\ 0 & 0 & 0 & 1 \\ 0 & a_{44} & 0 & 0 \end{bmatrix}$$

The system after adding control signals is:

$$\Delta\dot{\mathbf{x}} = (\mathbf{A} + \mathbf{BK})\Delta\mathbf{x} \tag{30}$$

If the value of $\mathbf{K}$ is appropriate, $\mathbf{A} + \mathbf{BK}$ can form a matrix to make the system asymptotically stable, and if $\mathbf{x}(0) \neq 0$, $\lim_{t\to\infty} \mathbf{x}(t) = 0$.

The eigenvalue of $\mathbf{A} + \mathbf{BK}$ is the pole of the regulator. If the pole of the regulator is located in the left half-plane of the s coordinate system, $\lim_{t\to\infty} \Delta\mathbf{x}(t) = 0$.

The problem of arranging the closed-loop poles to the desired position is called the pole arrangement. What should be noted is it's possible to modify any pole arrangement of the system only if the given system is entirely controllable.

There are four algorithms commonly used in pole placement of MIMO high-order systems. 1) Turn the multi-input system into a single-input system; 2) Convert the state space expression into the Laenberger controllable canonical form, and then the state feedback gain $\mathbf{K}$ can be solved; 3) Solve the $\mathbf{T}$ matrix of the Sylvester equation, if the $\mathbf{T}$ matrix is nonsingular, the $\mathbf{K}$ is obtained. 4) The state feedback gain $\mathbf{K}$ is obtained by the linear-quadratic optimal control method.

Comparing the four algorithms, the disadvantage of the first algorithm is that the single-input system generated by multi-input systemization is not unique, and the elements of the feedback gain matrix k_i calculated by this algorithm are often too large. The disadvantage of the second algorithm is that the calculation of the transformation matrix which can control the canonical form is tedious. The third algorithm cannot guarantee that the $\mathbf{T}$ matrix is nonsingular. The fourth algorithm is subjective in the balance between error and energy consumption, that is, the setting of the $\mathbf{Q}$ matrix and the $\mathbf{R}$ matrix.

In this paper, the state feedback matrix is obtained by taking the expected poles, and the logic of the control matrix is:

$$\Delta\mathrm{U} = \begin{bmatrix} k_{11}\Delta\omega_z + k_{12}\Delta\alpha + k_{13}\Delta\varphi + k_{14}\Delta I_\varphi \\ k_{21}\Delta\omega_z + k_{22}\Delta\alpha + k_{23}\Delta\varphi + k_{24}\Delta I_\varphi \end{bmatrix} \tag{31}$$

It can be seen that in the process of calculating elevator deflection components $\Delta\delta_z$, $k_{11}\Delta\omega_z$ and $k_{12}\Delta\alpha$ are differential terms and proportional terms; $k_{13}\Delta\varphi$ is flight-propulsion coupling term, and the fuel equivalence ratio error integral in $k_{14}\Delta I_\varphi$ has nothing to do with elevator adjustment, so $k_{14} = 0$.

Similarly, in the process of solving the command component $\Delta\varphi_c$ of fuel equivalence ratio, $k_{23}\Delta\varphi$ and $k_{24}\Delta I_\varphi$ are proportional terms and integral terms, $k_{22}\Delta\alpha$ is a coupling term, and $k_{21}\Delta\omega_z$ is an irrelevant term.

The fourth-order system is divided into a third-order system and a first-order system according to the logic of controlling attitude by elevator and controlling thrust by fuel equivalence ratio. The third-order system corresponds to the angle of attack control and has two dominant poles and one non-dominant pole. The dynamic index of the system step response is mainly determined by two dominant poles.

The damping ratio and natural frequency are calculated according to the performance index of the second-order system, and the dominant pole is selected using the formula (32). The relationship between adjustment time and overshoot and damping ratio and natural frequency is shown in formula (33):

$$s_{1,2} = -\xi\omega_n \pm \omega_n\sqrt{\xi^2 - 1} \tag{32}$$

$$\begin{cases} t_s = 4/(\xi\omega_n) \\ \xi = \dfrac{\ln(1/\sigma)}{\sqrt{\pi^2 + \left(\ln\frac{1}{\sigma}\right)^2}} \end{cases} \tag{33}$$

where ξ is called the damping ratio of the system; and ω_n , the undamped natural frequency. It is customary for the third pole to take a value more than 5 times the real part of the dominant pole. Considering the physical meaning of the state feedback matrix and the requirements of the system dynamic index, the position of the expected pole can be selected:

$$\begin{aligned} j_1 &= \lambda_1 + bi \\ j_2 &= \lambda_1 - bi \\ j_3 &= \lambda_2 \\ j_4 &= \lambda_3 \quad \lambda_1, \lambda_2, \lambda_3 < 0 \end{aligned}$$

The physical meaning of each element in matrix K is interpreted in detail. It is unreasonable to simply use the mathematical method to solve the matrix K because only four expected poles are used to establish the equation, while there are eight unknown elements, which leads to the non-unique solution of the matrix. The initial K matrix is a suitable value solved by combining the physical meaning of each element of the K matrix with engineering methods and $\mathrm{Re}[\lambda(\mathrm{A} + \mathrm{BK})] < 0$ can be guaranteed at this time. Under the influence of uncertainty in flight, some elements of matrix A may get changed, the corresponding elements of matrix K change as compensation, thus ensuring that the value of each element of A + BK remains unchanged. $\mathrm{Re}[\lambda(\mathrm{A} + \mathrm{BK})] < 0$ can be always held in this method. The iterative process is as Figure 6.

In the figure, λ is the iteration factor. c_i is the element value of matrix A + BK, and the adaptive control needs to ensure the constant value of c_i.

V. SIMULATION RESULTS

Select typical working conditions, and according to the transfer function calculated by formula 28, and the open-loop transfer function Bode diagram curves are given in Figure 5:

Based on the above dynamic model and controller, the simulation is carried out. The dynamic parameters of the aircraft are shown in Table 2:

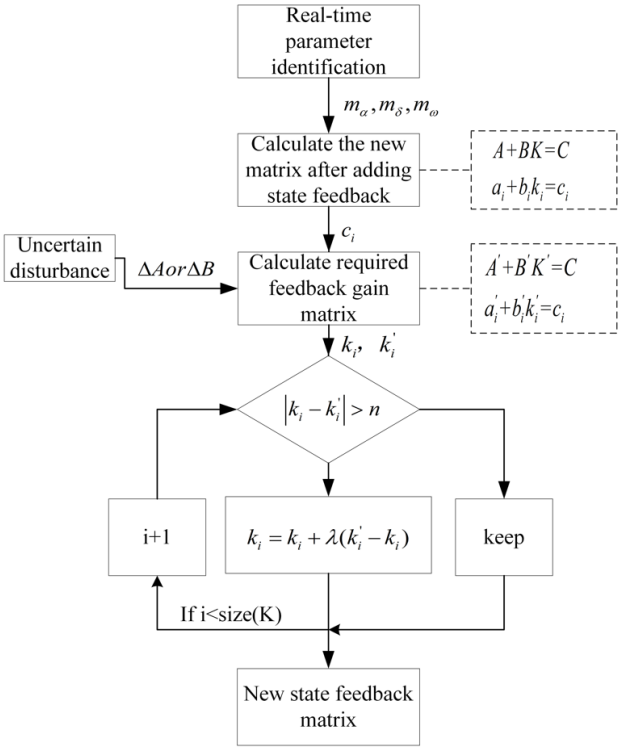

FIGURE 6. The gain update iteration flow.

TABLE 2. The ontological parameters of the hypersonic vehicle at wide-range Mach numbers.

Variable	Description	Value
c	Characteristic Length	6.938m
S	Reference area	60.32m^2
I_{yy}	Pitching moment of inertia	400701Nm
m	Mass	19000kg

According to the previous section, the desired pole is selected as:

$$\begin{aligned} j_1 &= -6.308 + 4.312i \\ j_2 &= -6.308 - 4.312i \\ j_3 &= -3.406 \\ j_4 &= -24 \end{aligned}$$

According to the formula (32-33), it is expected that the angle of attack setting time corresponding to this set of poles will be about 3.2 seconds, and the maximum overshoot will be about 20%.

Under the desired poles selected above and in combination with the requirements of the system dynamic response index, the tuning state feedback matrix is solved as $K = \begin{bmatrix} 8 & 40 & 0.1 & 0 \\ 0 & -0.2 & -1.5 & -0.5 \end{bmatrix}$. The flight process of the aircraft is set at an altitude of 25,000 meters and a speed of Mach 6. The initial angle of attack is 0 degrees and adjusted to 1 degree. The initial fuel equivalence ratio is 0, which is adjusted to 0.85 and simulated in the interval of 0 to 10

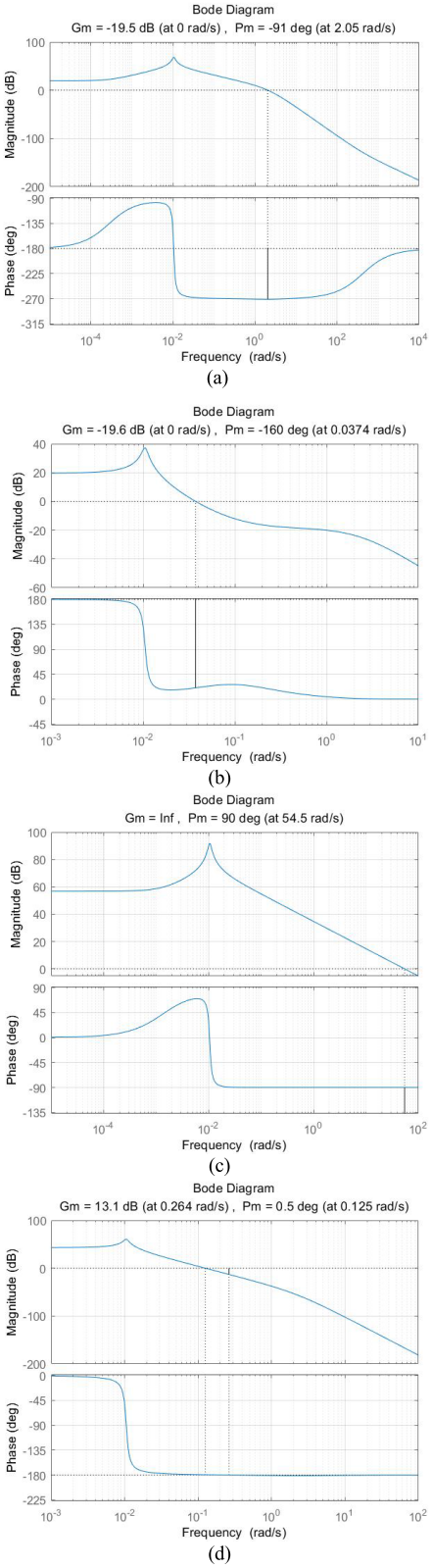

FIGURE 7. The Open-loop transfer function bode graph curve. (a) Bode diagram of the transfer function from the elevator to the angle of attack; (b) Bode diagram of equivalent ratio function from the elevator to Fuel equivalence ratio; (c) Bode diagram of the transfer function from Fuel equivalence ratio command to angle of attack; (d) Bode diagram of Fuel equivalence ratio command to Fuel equivalence ratio function.

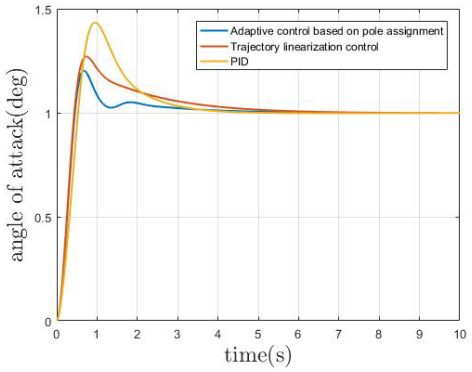

(a)

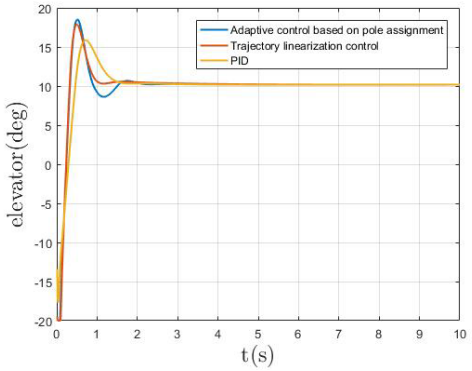

(b)

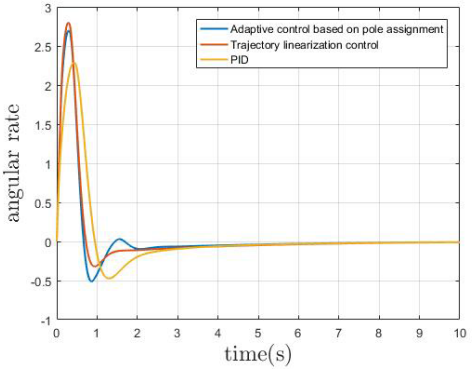

(c)

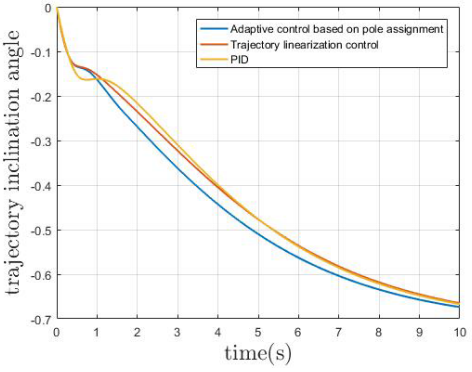

(d)

FIGURE 8. Adaptive gain adjustment control simulation curve of WIDE-RANGE VELOCITY VEHICLE. (a) The angle of attack control curve; (b) Elevator control curve; (c) Angular rate curve; (d) Trajectory inclination angle curve; (e) Pitch angle control curve.

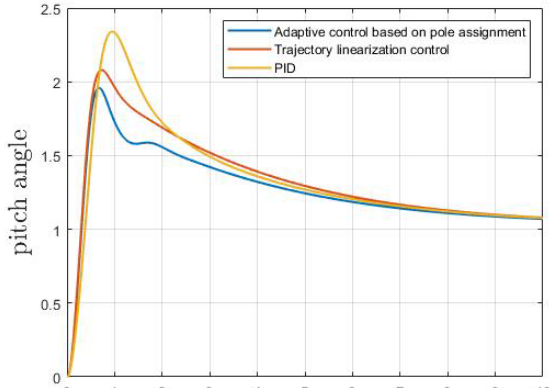

(e)

FIGURE 8. *(Continued.)* Adaptive gain adjustment control simulation curve of WIDE-RANGE VELOCITY VEHICLE. (a) The angle of attack control curve; (b) Elevator control curve; (c) Angular rate curve; (d) Trajectory inclination angle curve; (e) Pitch angle control curve.

TABLE 3. Dynamic performance comparison.

Variable	PID	TLC	Adaptive control based on pole assignment
Maximum overshot for angle of attack	43.4%	27.1%	20.2%
Setting time for angle of attack(s)	3.36	4.56	3.16
Maximum peak value of angular rate （deg/s）	2.286	2.795	2.696
Maximum peak value of pitch angle （deg）	2.341	2.696	1.959

seconds. The simulation results include the dynamic response process under normal conditions, dynamic response process of the elevator after adding 20% uncertainty, and dynamic response process of controller adaptive compensation while adding 20% uncertainty to the elevator. PID and trajectory linearization control (TLC) are simulated as comparative methods. The simulation results are shown in figure 8:

VI. DISCUSSIONS AND CONCLUSION

From Figure 7, due to the increase of the order of transfer function, the Bode diagram of the hypersonic vehicle at wide-range Mach numbers control system is more complex with the coupling of flight and propulsion. The amplitude of high-frequency band in (a) and (d) is small, which shows that the impaction from an executive body to the controlled objects (i.e., from the elevator to the angle of attack and from the fuel equivalence ratio command to the fuel equivalence ratio) has a strong ability to suppress noise. However, the high-frequency amplitude of the coupling control process as shown in (b) and (c) is large, which shows that they have a weak ability to suppress high-frequency noise. On the contrary, their low-frequency amplitude is higher, which shows that their steady-state is more accurate.

From Figure 8(a-b), the maximum overshoot of the PID control system for the angle of attack is 43.4%, and the setting time is 3.36 seconds Differ from PID, which linearizes the nonlinear system in only one working condition, LTC linearization in many different working conditions can reduce the overshoot of maximum angular velocity and angle of attack, which shows that it has certain advantages compared with PID. The maximum overshoot reduced to 27.1%, the setting time reach 2.89 seconds by LTC. Adaptive control based on desired pole assignment can adjust the controller according to the variation of the real-time flight parameter, which decrease the overshoot of angle of attack to 20.2%. The setting time is 3.16 seconds, which meets the requirements of the desired pole for the dynamic response index of the system. Results of simulation show that the adaptive controller can obviously improve the control quality of the system with uncertainties. From(c-e), although the adjustment time of the three cases is the same, it can be seen that the adaptive control can reduce the maximum peak value of the curve. It can be seen from c and d that the response curve of adaptive control is closer to the steady-state value as a whole.

In this paper, an adaptive controller based on pole assignment is adopted to suppress the disturbance caused by uncertainty in flight. Compared with the widely used methods such as trajectory linearization, the adaptive controller based on pole assignment can adjust the control parameters according to the real-time flight data identification, thus achieving a better integrated-control effect.

The hypersonic vehicle at wide-range Mach numbers model is built mainly according to the parametric method. On this basis, the detailed aerodynamic data and thrust data of the aircraft under various working conditions are calculated according to the panel method and the others, which can show a large proportion of the uncertainties and time variability in the large flight envelope. The flight-propulsion coupling characteristics of the hypersonic vehicle at wide-range Mach numbers are described by using the state-space equation and transfer function. On the basis of the simplified state-space equation, this paper gives an integrated control strategy for the hypersonic vehicle at wide-range Mach numbers by using the pole assignment method. Real-time identification based on flight data adjusts the controller parameters to compensate for the uncertain disturbance in flight while keeping the desired pole unchanged. The simulation results show that the pole assignment method can be used in the integrated control of the hypersonic vehicle at wide-range Mach numbers, and the influence of uncertain disturbance on the system during flight can be compensated by using the identification method. It shows that the adaptive controller based on the pole assignment is an effective in dealing with the coupling effect of flight and propulsion of the hypersonic vehicle at wide-range Mach numbers and the uncertainty in large flight envelope with low-complexity control framework.

Further research includes the following points:

(1) In this paper, the control of fuel equivalence ratio is simplified, and the dynamic process related to flight attitude is ignored. In the future, the dynamic process of fuel equivalence ratio can be analyzed and studied in more detail according to the parametric model;

(2) In terms of application objects, parametric models can be used for dynamic analysis of various aircraft. The adaptive control method based on pole assignment can be applied to the coupling control of MIMO systems in different fields;

(3) Empirical coupling control values are adopted in setting control coupling items, and identification of coupling can be added in the future to adjust coupling item parameters in real-time.

REFERENCES

[1] J. Liu, N.-F. Wang, J. Wang, and Z.-Y. Li, "Optimizing combustion performance in a solid rocket scramjet engine," *Aerosp. Sci. Technol.*, vol. 99, Apr. 2020, Art. no. 105560, doi: 10.1016/j.ast.2019.105560.

[2] L. Shi-Bin, "Design and optimization of aerodynamic configuration for the novel-concept vehicle with the wide-range Mach numbers," *J. Propuls. Technol.*, vol. 30, no. 6, pp. 735–739, 2009, doi: 10.3321/j.issn:1001-4055.2009.06.019.

[3] W. Jian-Li and Y. Yun-Feng, "Robust longitudinal flight controller design for the air-breathing hypersonic vehicle," in *Proc. IEEE Int. Symp. Knowl. Acquisition Model. Workshop*, Dec. 2008, pp. 494–497, doi: 10.1109/KAMW.2008.4810532.

[4] D. Zhang, S. Tang, Q.-J. Zhu, and R.-G. Wang, "Analysis of dynamic characteristics of the rigid body/elastic body coupling of air-breathing hypersonic vehicles," *Aerosp. Sci. Technol.*, vol. 48, pp. 328–341, Jan. 2016, doi: 10.1016/j.ast.2015.11.027.

[5] D. Zhang and S. Tang, "The propulsion/flight dynamics coupling analysis for air-breathing hypersonic vehicle," in *Proc. 4th Int. Conf. Intell. Hum.-Mach. Syst. Cybern.*, Aug. 2012, pp. 53–57, doi: 10.1109/IHMSC.2012.19.

[6] M. Mirmirani, M. Kuipers, J. Levin, and A. D. Clark, "Flight dynamic characteristics of a scramjet-powered generic hypersonic vehicle," in *Proc. Amer. Control Conf.*, 2009, pp. 2525–2532, doi: 10.1109/ACC.2009.5160500.

[7] M. A. Bolender and D. B. Doman, "Nonlinear longitudinal dynamical model of an air-breathing hypersonic vehicle," *J. Spacecraft Rockets*, vol. 44, no. 2, pp. 374–387, 2007, doi: 10.2514/1.23370.

[8] M. Brown, N. Mudford, A. Neely, and T. Ray, "Robust design optimization of two-dimensional scramjet inlets," in *Proc. 14th AIAA/AHI Space Planes Hypersonic Syst. Technol. Conf.*, 2006, p. 8140.

[9] S. E. Riddick, "An overview of NASA's learn-to-fly technology development," in *Proc. AIAA Scitech Forum*, 2020, p. 0760, doi: 10.2514/6.2020-0760.

[10] J. M. Brandon and E. A. Morelli, "Real-time onboard global nonlinear aerodynamic modeling from flight data," in *Proc. AIAA Atmos. Flight Mech. Conf.*, Atlanta, GA, USA, Jun. 2014, pp. 1–55.

[11] L. Liu, S. Dong, Y. J. Wang, and L. L. Ou, "Clearance of flight control law based on structural singular value theory," *IEEE Trans. Aerosp. Electron. Syst.*, vol. 51, no. 3, pp. 2138–2147, Jul. 2015, doi: 10.1109/TAES.2015.130822.

[12] C. Naigang, L. Hao, L. Baogang, and W. Changzhu, "Integrated technology of guidance and control for reusable aircraft," in *Proc. Symp. Space Electromech. Space Opt.*, 2017, pp. 55–61.

[13] S. E. Riddick, R. C. Busan, D. E. Cox, and S. A. Laughter, "Learn to fly test setup and concept of operations," in *Proc. Atmos. Flight Mech. Conf.*, Jun. 2018, p. 3308, doi: 10.2514/6.2018-3308.

[14] E. A. Morelli, "Autonomous real-time global aerodynamic modeling in the frequency domain," in *Proc. AIAA Scitech Forum*, Jan. 2020, p. 0761, doi: 10.2514/6.2020-0761.

[15] A. Mekky and O. R. Gonzalez, "LQ control for the NASA learn-to-fly free-to-roll project," in *Proc. IEEE Nat. Aerosp. Electron. Conf. (NAECON) Ohio Innov. Summit (OIS)*, Jul. 2016, pp. 173–178, doi: 10.1109/NAECON.2016.7856794.

[16] J. A. Grauer, "A learn-to-fly approach for adaptively tuning flight control systems," in *Proc. Atmos. Flight Mech. Conf.*, Jun. 2018, p. 3312, doi: 10.2514/6.2018-3312.

[17] J. Li, L. Zhuang, J. Song, C. Dong, and K. Guo, "An aerodynamic model identification method suitable for low-quality flight data," in *Proc. 3rd Int. Conf. Unmanned Syst. (ICUS)*, Nov. 2020, pp. 381–388, doi: 10.1109/ICUS50048.2020.9274990.

[18] J. Cui, J. Shi, Y. Li, S. Dong, X. Cui, and T. Huang, "Application of the variable weight combination model in aero-generator life prediction," in *Proc. Chin. Control Decis. Conf. (CCDC)*, May 2011, pp. 2970–2973, doi: 10.1109/CCDC.2011.5968761.

[19] A. Khalid, K. Zeb, and A. Haider, "Conventional PID, adaptive PID, and sliding mode controllers design for aircraft pitch control," in *Proc. Int. Conf. Eng. Emerg. Technol. (ICEET)*, Feb. 2019, pp. 1–6, doi: 10.1109/CEET1.2019.8711871.

[20] D. We, H. Xiong, and J. Fu, "Aircraft autopilot pitch control based on fuzzy active disturbance rejection control," in *Proc. Int. Conf. Ind. Informat.-Comput. Technol., Intell. Technol., Ind. Inf. Integr.*, Dec. 2015, pp. 144–147, doi: 10.1109/ICIICII.2015.119.

[21] S. Snyder, B. Bacon, E. A. Morelli, S. Frost, C. Teubert, and W. Okolo, "Online control design for learn-to-fly," in *Proc. Atmos. Flight Mech. Conf.*, Jun. 2018, pp. 1–27, doi: 10.2514/6.2018-3311.

[22] X. W. Bu and Q. Qi, "Fuzzy optimal tracking control of hypersonic flight vehicles via single-network adaptive critic design," *IEEE Trans. Fuzzy Syst.*, early access, Nov. 11, 2020, doi: 10.1109/TFUZZ.2020.3036706.

[23] X. W. Bu, Q. Qi, and B. Jiang, "A simplified finite-time fuzzy neural controller with prescribed performance applied to waverider aircraft," *IEEE Trans. Fuzzy Syst.*, early access, Jun. 14, 2021, doi: 10.1109/TFUZZ.2021.3089031.

[24] X. Bu, "Air-breathing hypersonic vehicles funnel control using neural approximation of non-affine dynamics," *IEEE/ASME Trans. Mechatronics*, vol. 23, no. 5, pp. 2099–2108, Oct. 2018, doi: 10.1109/TMECH.2018.2869002.

[25] H. Zhang, Y. Yu, H. Wang, and Y. Liu, "Reduced-order linear extended state observer based trajectory linearization control for hypersonic reentry vehicle under high maneuver flight with multiple disturbances," in *Proc. IEEE CSAA Guid., Navigat. Control Conf. (CGNCC)*, Aug. 2018, pp. 1–6, doi: 10.1109/GNCC42960.2018.9018888.

[26] H. Shen, Y. Liu, Y. Lu, D. Xiao, and B. Chen, "A parametric model for control integrated design of hypersonic vehicles," *Sci. Sinica Technol.*, vol. 46, no. 10, pp. 1024–1038, Oct. 2016, doi: 10.1360/N092016-00073.

[27] H. Shen, Y. Liu, B. Chen, and Y. Lu, "Control-relevant modeling and performance limitation analysis for flexible air-breathing hypersonic vehicles," *Aerosp. Sci. Technol.*, vol. 76, pp. 340–349, May 2018, doi: 10.1016/j.ast.2018.02.016.

[28] H.-D. Shen, R. Cao, Y.-B. Liu, F.-T. Jin, and Y.-P. Lu, "Control-oriented low-speed dynamic modeling and trade-off analysis of air-breathing aerospace vehicles," *J. Zhejiang Univ.-Sci. A*, vol. 20, no. 12, pp. 893–907, Dec. 2019, doi: 10.1631/jzus.A1900366.

[29] A. Ebrahimi-Fizik, E. Lakzian, and A. Hashemian, "Numerical investigation of wet inflow in steam turbine cascades using NURBS-based mesh generation method," *Int. Commun. Heat Mass Transf.*, vol. 118, Nov. 2020, Art. no. 104812, doi: 10.1016/j.icheatmasstransfer.2020.104812.

[30] J. Dang, T. Xie, H. Shao, and H. Song, "Research on adaptive NURBS interpolation algorithm for 3D engraving of manipulators," in *Proc. Int. Conf. Control, Robot. Intell. Syst. (CCRIS)*, 2020, pp. 32–36, doi: 10.26914/c.cnkihy.2020.045869.

[31] J. M. Vogel, A. G. Kelkar, G. Inger, C. Whitmer, A. Sidlinger, and A. Rodriguez, "Control-relevant modeling of hypersonic vehicles," in *Proc. Amer. Control Conf.*, 2009, pp. 2519–2524, doi: 10.1109/ACC.2009.5160682.

[32] J. Liu, Y. Hong, and Z. Xiong, "Simulation analysis of hypersonic vehicle flight control based on back-stepping and dynamic inversion," in *Proc. 33rd Chin. Control Conf.*, 2014, pp. 6358–6363, doi: 10.1109/ChiCC.2014.6896035.

[33] Y. Li, B. Chen, Y. Liu, and H. Shen, "Performance analysis of hypersonic vehicle based on aerodynamic derivatives," in *Proc. 36th Chin. Control Conf. (CCC)*, Jul. 2017, pp. 10370–10375, doi: 10.23919/ChiCC.2017.8029006.

[34] A. Kelkar, J. Vogel, G. Inger, C. Whitmer, A. Sidlinger, and C. Ford, "Modeling and analysis framework for early stage trade-off studies for scramjet-powered hypersonic vehicles," in *Proc. 16th AIAA/DLR/DGLR Int. Space Planes Hypersonic Syst. Technol. Conf.*, Oct. 2009, p. 7325, doi: 10.2514/6.2009-7325.

[35] Y. Yong, "Thereorical analysis, experimental study of scarmjet combustor operation process," Nat. Univ. Defense Technol., Changsha, China, Tech. Rep., 2004, doi: 10.7666/d.y789476.

[36] J. Dickeson, S. Sridharan, and A. Rodriguez, "Impact of plume modeling on the design and control for a class of air-breathing hypersonic vehicles," in *Proc. AIAA Guid., Navigat., Control Conf.*, Aug. 2011, p. 6229, doi: 10.2514/6.2011-6229.

[37] B. Han, H. Jiu, S. Pang, and J. Li, "Hydrothermal plume simulation for autonomous hydrothermal vent discovery," in *Proc. OCEANS*, 2012, pp. 1–7, doi: 10.1109/OCEANS-Yeosu.2012.6263527.

JIAXIN LI was born in Pingdingshan, Henan, China, in 1998. He received the B.S. degree in automation from the North China University of Water Resources and Electric Power, in 2020. He is currently pursuing the M.S. degree in aerospace science and technology with the Dalian University of Technology.

He has been a Research Assistant with the Key Laboratory of Advanced Technology for Aerospace Vehicles. His research interests include hypersonic vehicle guidance and control, and parametric model of hypersonic vehicle.

DANWEI LI received the B.S. and M.S. degrees in aircraft design from the Harbin Institute of Technology, in 2003 and 2009, respectively.

From 2009 to 2010, he worked with the Structural Department, Shenyang Aircraft Design and Research Institute, where he worked with the Flight Control Department, from 2010 to 2014, and has been working with the Aerospace Team, since 2014.

GUOQIANG WU received the B.S. degree in business administration, the M.S. degree in solid mechanics, and the Ph.D. degree in aircraft design from the Harbin Institute of Technology, in 2001, 2004, and 2009, respectively.

From 2009 to 2013, he was a Lecturer with the School of Aeronautics and Astronautics, Dalian University of Technology, where he has been an Assistant Professor, since 2013. His research interests include aircraft system simulation, and flight guidance and control.

KAI LIU received the B.S. degree in information and computing science from Jilin University, China, in 2007, and the Ph.D. degree from the Harbin Institute of Technology, China, in 2013.

He entered the 301 Research Institute, China Aerospace Third Research Institute, as an Aircraft Guidance and Control Engineer. Since 2017, he has been an Associate Professor with the Dalian University of Technology. His research interest includes flight guidance and control.